Tuning ferromagnetic $BaFe_2(PO_4)_2$ through a high Chern number topological phase

Young-Joon Song,[1] Kyo-Hoon Ahn,[1] Warren E. Pickett,[2,*] and Kwan-Woo Lee[1,3,†]
[1]*Department of Applied Physics, Graduate School, Korea University, Sejong 33019, Korea*
[2]*Department of Physics, University of California, Davis, California 95616, USA*
[3]*Department of Display and Semiconductor Physics, Korea University, Sejong 33019, Korea*
(Received 10 May 2016; published 20 September 2016)

There is strong interest in discovering or designing wide-gap Chern insulators. Here we follow a Chern insulator to trivial Mott insulator transition versus interaction strength U in a honeycomb-lattice Fe-based transition-metal oxide, discovering that a spin-orbit coupling energy scale $\xi = 40$ meV can produce and maintain a topologically entangled Chern insulating state against large band structure changes arising from an interaction strength U up to 60 times as large. Within the Chern phase the minimum gap switches from the zone corner K to the zone center Γ while maintaining the topological structure. At a critical strength U_c, the continuous evolution of the electronic structure encounters a gap closing then reopening, upon which the system reverts to a trivial Mott insulating phase. This Chern insulator phase of honeycomb lattice Fe^{2+} $BaFe_2(PO_4)_2$ corresponds to a large Chern number $\mathcal{C} = -3$ that will provide enhanced anomalous Hall conductivity due to the associated three edge states threading through the bulk gap of 80 meV.

DOI: 10.1103/PhysRevB.94.125134

I. BACKGROUND

The quantum anomalous Hall (QAH) insulator, also known as the Chern insulator, is a two-dimensional (2D) ferromagnetic (FM) insulator with a nonzero Chern number, resulting in a quantized boundary anomalous Hall conductivity without an external magnetic field as first proposed by the Haldane model on a hexagonal lattice [1]. The quantized conductivity is given by $\sigma_{xy} = \mathcal{C}(e^2/h)$ with the Planck constant h and electronic charge e, and the Chern number $\mathcal{C}$ quantized due to topological restrictions. $\mathcal{C}$, whose origin involves occupied states entangled with conduction states, corresponds to the number of dissipationless and gapless edge states for the FM 2D Chern insulator [2]. The QAH insulator is anticipated to be a good candidate, with a great advantage in practice, for anticipated applications of no energy consumption electronics [2], for Majorana fermions and their manipulation [3], and for future photonic devices [4]. High Chern number materials will provide comparably higher conductivities.

A Chern insulating state arises in a broken time reversal system where spin-orbit coupling (SOC) inverts valence and conduction bands which would otherwise provide a trivial insulating phase. The topological gap is thereby limited by the strength of SOC. The interplay between strong interactions and strength of SOC is being explored in the contexts of topologically insulating iridates [5] and possibly osmates, but primarily model Hamiltonian treatments have explored (or suggested) the related phase diagram, and none have followed how the phase transition occurs. Witczak-Krempa and collaborators [6] have presented a heuristic phase diagram in which a Chern insulating state borders a (trivial) Mott insulator. However, modeling of the evolution of a realizable system through such a transition is only now being addressed, with an example being the results of Doennig and coworkers [7] of the interplay between SOC and correlation effects in manipulating the competition between Chern and Mott phases in a buckled (111) bilayer of $LaFeO_3$ in $LaAlO_3$. Here we provide a related example for the bulk transition-metal oxide and Ising FM $BaFe_2(PO_4)_2$ (BFPO), whose structure is shown in Fig. 1, of the competition between SOC and strong interaction in creating and then annihilating a high Chern number QAH phase.

The QAH phase has been predicted in various artificial structures that can be roughly classified into three groups: (1) topological insulators doped by magnetic transition-metal (TM) ions [8–10], (2) thin TM layers on a hexagonal lattice [11,12], and (3) heterostructures of {111}-oriented double-perovskite or TM oxides [7,13–15]. A QAH state of $\mathcal{C} = \pm 2$ was calculated for CrO_2/TiO_2 [14] and VO_2/TiO_2 [15] heterostructures. However, having gaps of 2–4 meV leaves them primarily of academic interest. A QAH state was also suggested and then calculated for perovskite bilayers [7,13], but required a tuning of hybridization or trigonal distortion to realize a QAH phase. Zhang *et al.* suggested $\mathcal{C} = \pm 2$ QAH with a larger (∼100 meV) gap in graphene decorated with 5*d* transition-metal ions [11], while Zhou *et al.* proposed the $\mathcal{C} = 1$ state with a larger gap around 100 meV in a hexagonal tungsten lattice on the monolayer Cl-covered Si(111) surface [12]. Generally, the QAH phase in these thin films has been expected only at a particular thickness. Beyond the predicted systems, toy models [16–18] with topological flat bands have suggested high Chern numbers in thin films or artificial heterostructures. A Chern insulating state in bulk solids remains a goal for both research study and possible applications, and large Chern numbers are especially valued.

Aside from these theoretically designed systems, a QAH realization has been reported in the Cr-doped topological insulator $(Bi,Sb)_2Te_3$ with $\mathcal{C} = 1$ at very low temperature [19]. To realize a QAH insulator with a large nontrivial gap, high Curie temperature T_C, and high Chern number in real or easily synthesized compounds remains a challenge. Morimoto and Nagaosa proposed [20], based on a strong forward-scattering

*pickett@physics.ucdavis.edu
†mckwan@korea.ac.kr

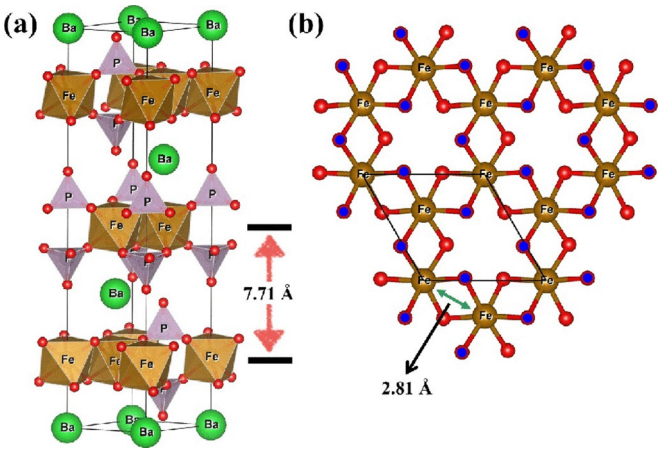

FIG. 1. The rhombohedral structure of $BaFe_2(PO_4)_2$ (left panel), consisting of honeycomb sublattices of FeO_6 octahedra (right panel, top view) and intervening PO_4 tetrahedra and Ba^{2+} ions. The primitive cell (solid lines in the right panel) contains two Fe^{2+} ions. The inter- and intralayer Fe-Fe distances, indicating highly 2D character, are provided.

amplitude model, that large-gap topological insulators may be possible to achieve in strongly interacting systems, which shifts the focus away from *s-p* materials.

In this paper we uncover, and then analyze the nature of, a transition between gapped topological (Chern) and trivial (Mott) insulating states in BFPO using a correlated band approach including SOC, by tuning the interaction strength. With increasing interaction strength, a compensated low-density Chern semimetal evolves into a $\mathcal{C} = -3$ Chern insulator with a gap up to 80 meV, then transforms abruptly to a trivial Mott insulator, versus increasing strength of on-site Coulomb repulsion U. It is remarkable that the critical value for the transition is $U_c = 2.45$ eV, a factor of more than sixty greater than the SOC strength $\xi = 40$ meV that produced the Chern phase. This interplay between SOC and strong interaction highlights how small energy scales can leverage topological restrictions to resist effects of much larger energy scales.

II. STRUCTURE, SYMMETRY, METHODS

A. Structure and symmetry

Symmetries that are present can be critical for topological materials. Insulating BFPO [21] crystallizes in space group $R\bar{3}$ (threefold rotation plus inversion) and is composed of layered 2D honeycomb sublattices of Fe^{2+} ions within FeO_6 octahedra, as pictured in Fig. 1. Due to a substantial interlayer separation of the Fe layers separated by Ba^{2+} and $(PO_4)^{3-}$ insulating layers, BFPO is 2D electronically. BFPO was synthesized by Mentré and coworkers [22,23], who identified the rare 2D Ising FM nature with Curie temperature $T_C = 65$ K. The very large calculated magnetocrystalline anisotropy is related to the large orbital moment. Our previous study [21] provided the relaxed atomic positions and revealed large exchange splitting $\Delta_{ex} = 3$ eV of the d^6 ion, enforcing the high-spin $S = 2$ configuration with its filled and inactive majority d orbitals. SOC will couple the single minority t_{2g} electron to majority orbitals 2–3 eV removed in energy. Nevertheless, as we will see, SOC plays a critical role in BFPO.

B. Theoretical methods

The all-electron full-potential code WIEN2K [24] incorporating density-functional-theory-based methods was applied, with the structural parameters optimized in our previous study [21]. The Perdew-Burke-Ernzerhof generalized gradient approximation (GGA) was used as the exchange-correlation functional [25]. The combined effects of correlation (Hubbard U) and SOC, needed to produce the insulating state, were included through GGA+U+SOC calculations. Based on previous experience [21], U is varied up to 4 eV, while the Hund's exchange parameter J is fixed to 0.7 eV.

From these results, a tight-binding Hamiltonian for the t_{2g} manifold was obtained in terms of maximally localized Wannier functions [26] as implemented in WANNIER90. All necessary files for WANNIER90 were prepared by the code WIEN2WANNIER [27]. The Brillouin zone (BZ), gapped almost everywhere, was sampled by $11 \times 11 \times 11$ k mesh, and 16 orbitals were used for the Wannier function projection. Using WANNIER90, the Berry curvature and the anomalous Hall conductivity were calculated with a very dense k-point grid of 5×10^5 points to picture the Berry curvature and $300 \times 300 \times 300$ integration mesh to evaluate the anomalous Hall conductance.

III. RESULTS AND ANALYSIS

A. Band structure and Berry curvature

First we address the evolution of the band structure and Berry curvature $\Omega_z(\vec{k})$ versus increasing strength of U, finding unanticipated behavior. Although the perturbation theory expression for Ω_k is used in the calculation, it is instructive to note the expression in terms of the periodic part of the Bloch function $u_k = w_k \exp(i\gamma_k)$ with non-negative magnitude w_k and real phase γ_k (band indices suppressed),

$$\Omega_k = -i \sum_{ij} \epsilon_{ij} \langle \partial_{k_i} u_k | \partial_{k_j} u_k \rangle$$
$$= 2\big[\langle \partial_{k_x} w_k | w_k \partial_{k_y} \gamma_k \rangle + (x \leftrightarrow y)\big], \quad (1)$$

where ϵ_{ij} is the rank-2 antisymmetric unit tensor. The usual expression from perturbation theory suggests (as we find) that regions with small band gaps are important [15,28]. These regions of small gap may also involve larger matrix elements, because mixing by SOC is larger when the gap is smaller.

Equation (1) makes explicit that a nonvanishing Berry curvature requires a k-dependent phase. More specifically, it provides a different picture than the perturbation theory expression (which is what is actually evaluated). The complementary interpretation is that the Berry curvature obtains large contributions from where the gradients of both w_k and γ_k are large. Evidently small gaps and large velocity matrix elements promote such large gradients. In integer quantum Hall effect systems the Chern number was related to zeros in u_k [29].

In the uncorrelated limit $U = 0$, a tiny electron pocket in the Dirac point valley at K, visible in Fig. 2(a), is compensated with a hole pocket at Γ [21], preventing the Dirac point from

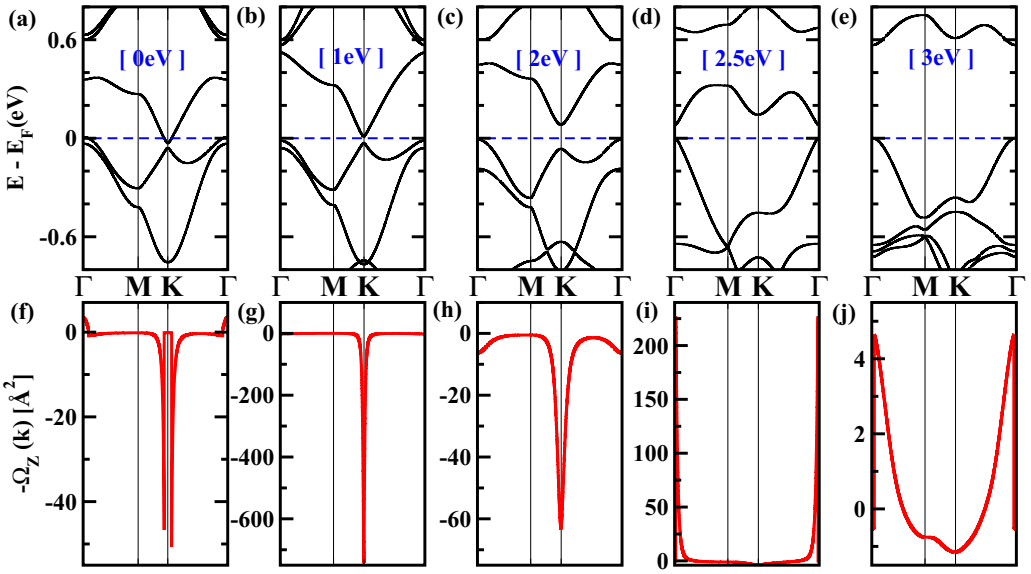

FIG. 2. Top row: GGA+SOC+U band structures versus U, near the gap around zero energy. Two occupied minority bands lie below $E_F = 0$. Bottom row: Berry curvatures Ω_k along the Γ-M-K-Γ lines, also versus U. Note the different scales and signs of the vertical axes in the Ω_k plots. The origin of structure in Ω_k is described in the text.

pinning E_F. SOC leads to the opening of a gap of 40 meV between the Dirac bands at K, providing the SOC energy scale [30] $\xi = 40$ meV. The small gap results in sharp peaks appearing in Fig. 2(f) in the curvature $\Omega_z(\vec{k})$ near the two K points; the splitting into two sharp peaks is caused by the Fermi level overlapping slightly the conduction band, reproduced correctly by the fine k-point integration mesh.

B. Evolution with interaction strength

For U as small as 1 eV the band overlap disappears, the Dirac point pins the Fermi energy as in graphene, and a sharp, almost δ-function-like peak appears in $\Omega_z(\vec{k})$ at K, shown in Fig. 2(g). Unlike in graphene, here an orbital degree of freedom is involved. The Dirac point degeneracy reflects the degeneracy in $R\bar{3}$ symmetry of the e'_g orbitals, the bands being linear combinations of Fe orbitals with opposite orbital moment projections. Incorporating SOC, these orbitals become entangled with the unbalanced spin character, and a gap of several tens of meV is opened at K without inducing any significant orbital moment; i.e., e'_g occupation is retained.

With further increase in U, the peaks in $\Omega_z(\vec{k})$ broaden as the band structure evolves, with the gap at K increasing smoothly without significant orbital moment. For U up to a critical value U_c, SOC retains its hold on the Chern state (see below), in spite of the large value of U and of spin-exchange splitting Δ_{ex}, compared to ξ. The bands and Berry curvature calculated for values of U from 2.40 eV to 2.475 eV are shown in Fig. 3. Above $U = 2$ eV the gap between valence and conduction bands at Γ decreases rapidly, closing at the critical value $U_c = 2.45$ eV as shown in Fig. 4, lower panel. This gap closing and reopening marks a disentanglement of bands and loss of topological character, as we verify below. Note that the eigenvalue crossing at Γ does not lead to a metallic trivial state, but to a Mott insulating state dictated by the Coulomb repulsion U. The vanishing of the Chern number at the transition suggests that the character of the Wannier functions of the two filled bands will have changed discontinuously at the critical point. The character of the Berry curvature changes dramatically, as shown in Fig. 5.

We had previously found [21] that beyond $U \approx 2.5$ eV the orbital moment m_ℓ increases rapidly from ~0.1 μ_B to 0.5–0.6 μ_B, asymptoting to the remarkably large value (for a $3d$ ion) of 0.7 μ_B for $U > 5$ eV. This evolution reflects a reoccupation of orbitals. In the Chern phase the minority t_{2g} electron is in a linear combination with almost equal amounts of orbital component $m_\ell = \pm 1$ and perhaps some $m_\ell = 0$, while beyond U_c the $m_\ell = +1$ orbital becomes fully occupied. The spin remains close to its $S = 2$ value. This jump in orbital moment signals the reoccupation from a linear combination of the two e'_g orbitals to dominant occupation of the complex $m_\ell = +1$ linear combination, a sign that SOC retains influence even after the loss of topological character. The topological-to-trivial transition thus results from a continuous, strong-interaction-driven band reordering, manipulated by the interplay between U and the SOC energy $\xi = 40$ meV. The transition occurs at a ratio $U/\xi = 60$.

C. Chern number and its origin

A chemical-potential-resolved Chern number $\mathcal{C}(E)$ is obtained from the anomalous Hall conductivity $\sigma_{xy} = \mathcal{C}e^2/h$ by integrating the Berry curvature Ω_k over the zone, up to the chemical potential. For values of U increasing through U_c, the energy-resolved $\sigma_{xy}(E)$ near E_F is displayed in the top panel of Fig. 4. The bottom panel of this figure shows the evolution of the gap, increasing from zero at $U = 0$ and achieving 80 meV at $U = 2$ eV. In the range $U = 2.0$–2.4 eV the minimum gap moves from its position at K to Γ. In this range BFPO is a Chern insulator with $\mathcal{C} = -3$, signaling a quantum anomalous Hall phase with *three times* the minimum quantized anomalous Hall conductivity. Rapidly with U increasing from 2.40 eV, the

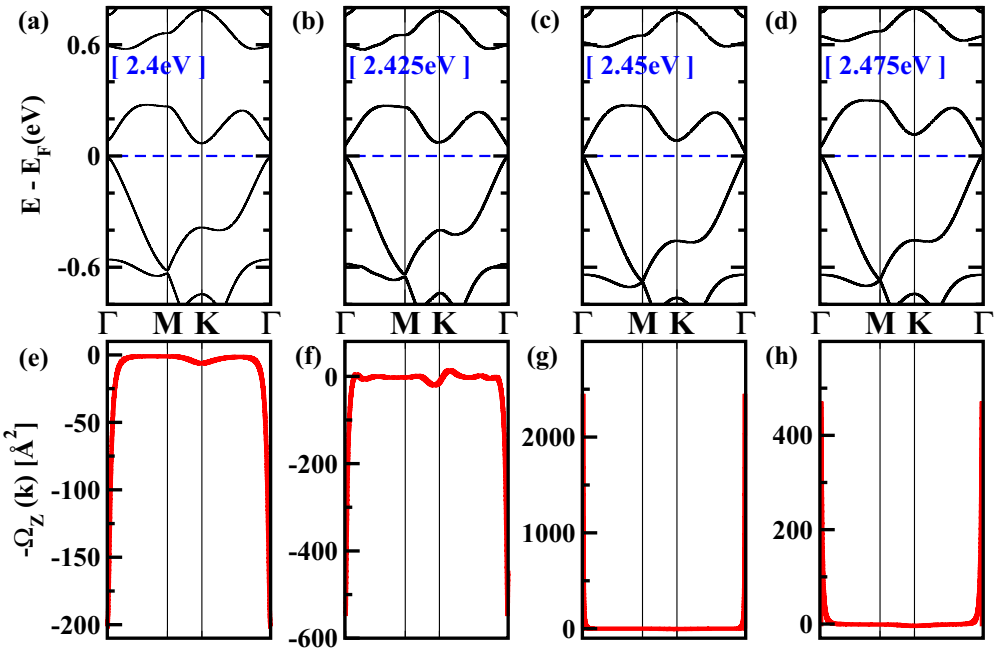

FIG. 3. As in Fig. 2, but for U approaching U_c on a fine scale. The regime $U > U_c$ [panels (c) and (d)] after band disentanglement (which occurs at Γ, not at K) provides the nontopological phase in which the Mott gap increases from zero and the orbital moment increases rapidly. Note that the Berry curvature changes its predominant sign at U_c (as well as integrating to zero).

gap at Γ closes and reopens due to the interchange in energy of the two bands at Γ. At $U = 2.5$ eV, the contribution of the very sharp positive peak at Γ is canceled by smaller negative contributions elsewhere, and $\mathcal{C} \to 0$; BFPO has transformed to a trivial insulator.

Besides the fundamental gap, there are additional nontrivial gaps at higher energies. The right panel of Fig. 6 shows σ_{xy} in the −0.25 eV to 1.5 eV range for $U = 2$ eV. Overall, there are three nontrivial gaps, about 80 meV wide at E_F and 100 meV at 0.5 eV, and a smaller gap at 1.3 eV. Notably, the highest band has $\mathcal{C} = -6$, while the two bands just below provide $\mathcal{C} = +9$ to the running sum. Strong spin-orbit entanglement extends throughout the t_{2g} bands in the Chern phase. The nontrivial states can be attributed to topological spin-orbit band entanglement, at the K points for the physical, fundamental gap; at the Γ point for band filling up to 0.5 eV; again at the K points for band filling to 1.3 eV (see the left panel of Fig. 6). Above U_c, the last two gaps increase a little, whereas the lowest one becomes trivial.

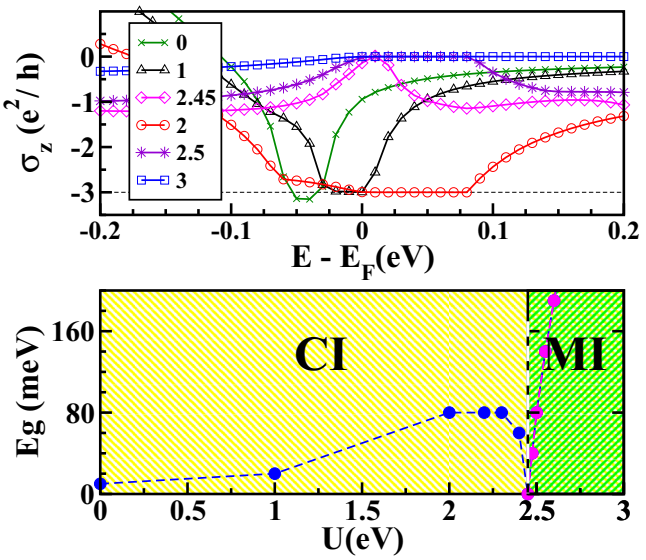

FIG. 4. Top panel: Anomalous Hall conductance σ_{xy} in units of e^2/h versus chemical potential, for the range of $U = 0$–3 eV. Below $U_c = 2.45$ eV, a nontrivial gap ∼0.1 eV with Chern number of −3 appears, due to the spin-orbit driven gap at the K points. Bottom panel: The minimum direct gap versus repulsion strength U. The Chern insulator (CI) phase persists up to U_c; the minimum direct gap shifts from K to Γ around $U = 2.2$ eV. Above U_c lies the Mott insulator (MI) phase, where the gap increases rapidly with U to nearly 0.5 eV at $U = 4$ eV.

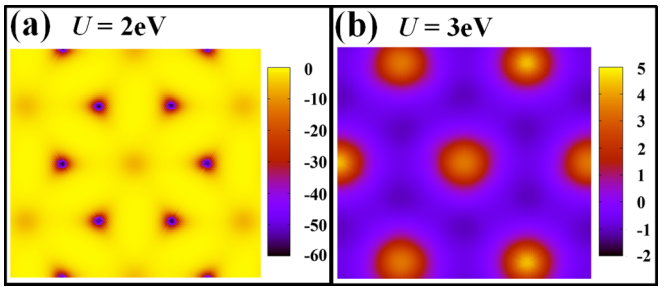

FIG. 5. Berry curvature Ω_k in the entire zone. Left panel: $U = 2$ eV, in the Chern phase ($\mathcal{C} = -3$), where strong peaks occur at the K points. Right panel: $U = 3$ eV, the $\mathcal{C} = 0$ trivial phase. Positive values of Ω_k around the Γ point are canceled by negative values throughout the rest of the zone.

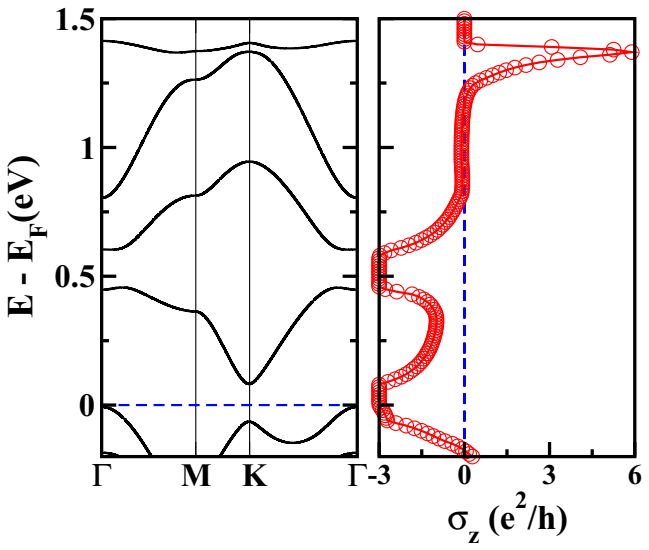

FIG. 6. Enlarged GGA+SOC+U band structures (left) and energy-resolved anomalous Hall conductance σ_{xy} (right) in units of e^2/h at $U = 2$ eV. The two bands below the gap (horizontal line; one band is not visible) provide $\mathcal{C} = -3$; the next higher band is nontopological $\Delta\mathcal{C} = 0$; entanglement of the top band with the next lower one gives it a very large Chern number $\mathcal{C} = 6$.

IV. ANGULAR MOMENTA AND THEIR TEXTURES

SOC produces noncollinear texture of the spin and orbital magnetizations, as studied early on in real space by Nordström and Singh [31]. Here we study the spin and orbital moment texture in k space, comparing its behavior in the Chern insulator phase to that in the Mott insulator phase. The results indicate effects of spin-orbit coupling can be strongly confined to specific regions of the zone, but in a manner very different from the high but narrow peaks of the Berry curvature.

The contribution to the orbital moment (and analogously for the spin moment) at point $\vec{r}$ from point $\vec{k}$ in the zone is

$$m_k^{\ell}(\vec{r}) = \sum_n^{occ} u_{k,n}^*(\vec{r})\vec{l}u_{k,n}(\vec{r}), \tag{2}$$

in terms of the two occupied minority band wave functions $u_{k,1}$ and $u_{k,2}$. These quantities can be summed over the zone to give the texture in real space, or integrated over the cell to give the texture in the zone. It is this latter approach that we address here, since topological character is connected directly to the $\vec{k}$ dependence of the Bloch functions.

With the hope of uncovering additional aspects of the nature of the topological transition, we present in Fig. 7 the orbital moment $\sum_n \langle u_{k,n}|\vec{l}|u_{k,n}\rangle$ and spin $\sum_n \langle u_{k,n}|\vec{s}|u_{k,n}\rangle$ textures summed over the two occupied minority bands, which are the orbitally active ones in the t_{2g} manifold. The band-decomposed analogs are presented in the Supplemental Material [32]. One can readily see that the texture is highly structured, compared for example to the simple vortex shape found on Cu(111) and Au(111) surfaces by Kim *et al.* [33].

In the Chern phase $U < U_c$ (left panels of Fig. 7) both orbital and spin textures are slowly varying near their mean values except for sharply defined elliptical regions around the K and K' points, where a significant disruption appears. Most notably, the orbital texture displays chiral character of

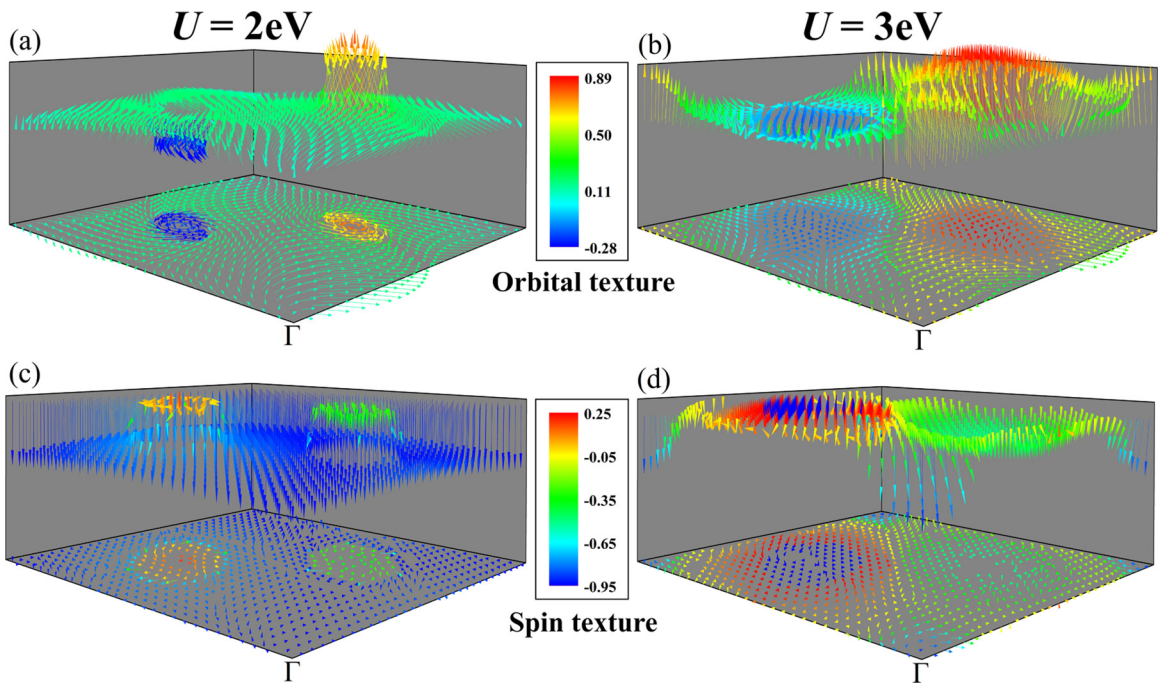

FIG. 7. Orbital $\sum_n \langle u_{kn}|\vec{l}|u_{kn}\rangle$ and spin $\sum_n \langle u_{kn}|\vec{s}|u_{kn}\rangle$ textures in a square region in $\vec{k}$ space. The axes are along Cartesian axes; Γ is at the near corner, M is midway along the diagonal toward the far corner, the vortices circle the K, K' points. (a) The orbital texture in the Chern phase ($U = 2$ eV) and (b) in the $U = 3$ eV trivial Mott insulator. (c), (d) The corresponding spin textures. The color denotes the $\hat{z}$ component of the texture field, with positive being parallel to the spin orientation, i.e., $\hat{c}$ direction, while the arrow provides the direction. The bottom plane provides the $\hat{z}$ projection to allow better visualization of the in-plane variation.

oppositely oriented circulations, reminiscent of the source-sink character found in the Berry connection in honeycomb lattice models. The spin is large everywhere, consistent with the ferromagnetic character, with texture that also displays well-defined, but different size and shape, regions around the K and K' points. The z components differ in the two regions, both being substantially different from the mean.

Beyond the critical value U_c, the Mott insulating state appears with enhanced $m_\ell = +1$ character throughout the zone. There is a small orbital moment $\sim 0.1\ \mu_B$ for $U < U_c$ but it increases rapidly at larger U. The corresponding textures are shown in the right panels of Fig. 7. The transition from Chern to Mott insulator at U_c is accompanied by a change in character of both orbital and spin texture fields. Now the effect of SOC in coupling spin texture to orbital texture dies rather abruptly away from the K, K' points, and structure has appeared around Γ.

It should be mentioned that, unlike the Chern number, the change between the textures at $U = 2$ eV and $U = 3$ eV is, from its definition, not abrupt. The value of the (say) orbital field $\sum_n \langle u_{k,n}|\vec{l}|u_{k,n}\rangle$ at one point $\vec{k}$ does not know what is occurring at other k points, nor does it know specifically about global topological properties; it varies continuously with changes, including changes in U, as long as no first-order transition is encountered.

Some general observations can be made. A strictly local isotropic atomic moment should correspond to a smooth, symmetric texture in k space. This is not observed, so the Fe moment has substantial itinerant character. A uniform (purely itinerant) magnetization in real space would arise from a strong peak at small $|k|$. This also is not observed, so the Fe moment does have substantial local character. It might also be relevant that the Fe moment is calculated to have extremely large magnetocrystalline anisotropy. The sharp boundaries of regions differing from featureless texture are much more prominent in the Chern phase than in the trivial phase, indicating that real-space texture evolves in both the orbital and spin moments as the orbital moment becomes larger and better defined.

V. SUMMARY

In this work we have followed the evolution of the honeycomb lattice Ising ferromagnet $BaFe_2(PO_4)_2$ from Chern insulator at small to moderate interaction strength U to the Mott insulator phase beyond the critical strength $U_c = 2.45$ eV, the latter being the physical regime. A noteworthy aspect is that the Chern phase has $\mathcal{C} = -3$ and, at its maximum, a sizable gap of 80 meV. For small U after SOC is included, the Chern insulator phase is obtained within which the gap at K increases very slowly with U. The small SOC strength $\xi = 40$ meV is sufficient to withstand increasing U and support the topological phase up to the critical value $U_c = 2.45$ eV. This support is possible because the increasing (with U) gap at K is supplanted by a decreasing gap at Γ. However, the gap at Γ closes rapidly, and immediately reopens with the system in a trivial Mott insulating phase ($\mathcal{C} = 0$). For Fe in an oxide insulator, U will be at least 4–5 eV in magnitude, so we do not expect $BaFe_2(PO_4)_2$ to show Chern insulating properties. Evidently a larger strength of SOC or smaller U is the direction to search for a Chern insulator in this class.

For additional insight, we have demonstrated that the spin and angular momentum textures throughout the zone experience an evolution from a tight structure around the K and K' points in the Chern phase to a more extended character in the Mott phase, varying more smoothly throughout the zone.

A distinctive feature of BFPO is the large Chern number $\mathcal{C} = -3$. In fact, the highest lying minority t_{2g} band has $\mathcal{C} = -6$, with the intermediate bands contributing $\mathcal{C} = +9$. Ren *et al.* [34] in their review have commented on large Chern number systems, and referenced the few that have been predicted, mostly in model systems. As an example, Jiang *et al.* [35] have calculated Chern numbers for multilayer films in magnetic fields for which the Chern number, for tuned field values, can be as large as the number of layers (up to 12 in their model).

ACKNOWLEDGMENTS

We acknowledge A. S. Botana for technical discussions, A. Essin and K. Park for conversations on topological insulators, J. Kuneš for assistance on angular momentum texture, and R. Pentcheva for discussions of related behavior in buckled (111) transition-metal oxide bilayers. This research was supported by National Research Foundation of Korea Grants No. NRF-2013R1A1A2A10008946 and No. NRF-2016R1A2B4009579 at Korea University, and by US Department of Energy Grant No. DE-FG02-04ER46111 (W.E.P.).

[1] F. D. M. Haldane, Model for a Quantum Hall Effect without Landau Levels: Condensed-Matter Realization of the "Parity Anomaly", Phys. Rev. Lett. **61**, 2015 (1988).

[2] For a review, see H. Weng, R. Yu, X. Hu, X. Dai, and Z. Fang, Quantum anomalous Hall effect and related topological electronic states, Adv. Phys. **64**, 227 (2015).

[3] S. R. Elliott and M. Franz, Majorana fermions in nuclear, particle, and solid-state physics, Rev. Mod. Phys. **87**, 137 (2015).

[4] S. A. Skirlo, L. Lu, and M. Soljačić, Multimode One-Way Waveguides of Large Chern Numbers, Phys. Rev. Lett. **113**, 113904 (2014).

[5] J.-M. Carter, V. V. Shankar, M. A. Zeb, and H.-Y. Kee, Semimetal and topological insulator in perovskite iridates, Phys. Rev. B **85**, 115105 (2012).

[6] W. Witczak-Krempa, G. Chen, Y. B. Kim, and L. Balents, Correlated quantum phenomena in the strong spin-orbit regime, Annu. Rev. Condens. Matter Phys. **5**, 57 (2014).

[7] D. Doennig, S. Baidya, W. E. Pickett, and R. Pentcheva, Design of Chern and Mott insulators in buckled 3*d*-oxide honeycomb lattices, Phys. Rev. B **93**, 165145 (2016).

[8] C.-X. Liu, X.-L. Qi, X. Dai, Z. Fang, and S.-C. Zhang, Quantum Anomalous Hall Effect in $Hg_{1-y}Mn_yTe$ Quantum Wells, Phys. Rev. Lett. **101**, 146802 (2008).

[9] R. Yu, W. Zhang, H.-J. Zhang, S.-C. Zhang, X. Dai, and Z. Fang, Quantized anomalous Hall effect in magnetic topological insulators, Science **329**, 61 (2010).

[10] C. Fang, M. J. Gilbert, and B. A. Bernevig, Large-Chern-Number Quantum Anomalous Hall Effect in Thin-Film Topological Crystalline Insulators, Phys. Rev. Lett. **112**, 046801 (2014).

[11] H. Zhang, C. Lazo, S. Blügel, S. Heinze, and Y. Mokrousov, Electrically Tunable Quantum Anomalous Hall Effect in Graphene Decorated by 5*d* Transition-Metal Adatoms, Phys. Rev. Lett. **108**, 056802 (2012).

[12] M. Zhou, Z. Liu, W. Ming, Z. Wang, and F. Liu, sd^2 Graphene: Kagome Band in a Hexagonal Lattice, Phys. Rev. Lett. **113**, 236802 (2014).

[13] A. M. Cook and A. Paramekanti, Double Perovskite Heterostructures: Magnetism, Chern Bands, and Chern Insulators, Phys. Rev. Lett. **113**, 077203 (2014).

[14] T. Cai, X. Li, F. Wang, S. Ju, J. Feng, and C.-D. Gong, Single-spin Dirac fermion and Chern insulator based on simple oxides, Nano Lett. **15**, 6434 (2015).

[15] H. Huang, Z. Liu, H. Zhang, W. Duan, and D. Vanderbilt, Emergence of a Chern-insulating state from a semi-Dirac dispersion, Phys. Rev. B **92**, 161115(R) (2015).

[16] F. Wang and Y. Ran, Nearly flat band with Chern number $C = 2$ on the dice lattice, Phys. Rev. B **84**, 241103(R) (2011).

[17] M. Trescher and E. J. Bergholtz, Flat bands with higher Chern number in pyrochlore slabs, Phys. Rev. B **86**, 241111(R) (2012).

[18] S. Yang, Z.-C. Gu, K. Sun, and S. Das Sarma, Topological flat band models with arbitrary Chern numbers, Phys. Rev. B **86**, 241112(R) (2012).

[19] C.-Z. Chang, J. Zhang, X. Feng, J. Shen, Z. Zhang, M. Guo, K. Li, Y. Ou, P. Wei, L.-L. Wang, Z.-Q. Ji, Y. Feng, S. Ji, X. Chen, J. Jia, X. Dai, Z. Fang, S.-C. Zhang, K. He, Y. Wang, L. Lu, X.-C. Ma, and Q.-K. Xue, Experimental observation of the quantum anomalous Hall effect in a magnetic topological insulator, Science **340**, 167 (2013).

[20] T. Morimoto and N. Nagaosa, Weyl Mott insulator, Sci. Rep. **6**, 19853 (2016).

[21] Y.-J. Song, K.-W. Lee, and W. E. Pickett, Large orbital moment and spin-orbit enabled Mott transition in the Ising Fe honeycomb lattice $BaFe_2(PO_4)_2$, Phys. Rev. B **92**, 125109 (2015).

[22] R. David, A. Pautrat, D. Filimonov, H. Kabbour, H. Vezin, M.-H. Whangbo, and O. Mentré, Across the structural re-entrant transition in $BaFe_2(PO_4)_2$: Influence of the two-dimensional ferromagnetism, J. Am. Chem. Soc. **135**, 13023 (2013).

[23] H. Kabbour, R. David, A. Pautrat, H.-J. Koo, M.-H. Whangbo, G. André, and O. Mentré, A genuine two-dimensional Ising ferromagnet with magnetically driven re-entrant transition, Angew. Chem. Int. Ed. **51**, 11745 (2012).

[24] K. Schwarz and P. Blaha, Solid state calculations using WIEN2k, Comput. Mater. Sci. **28**, 259 (2003).

[25] J. P. Perdew, K. Burke, and M. Ernzerhof, Generalized Gradient Approximation Made Simple, Phys. Rev. Lett. **77**, 3865 (1996).

[26] A. A. Mostofi, J. R. Yates, Y.-S. Lee, I. Souza, D. Vanderbilt, and N. Marzari, wannier90: A tool for obtaining maximally-localised Wannier functions, Comput. Phys. Commun. **178**, 685 (2008).

[27] J. Kuneš, R. Arita, P. Wissgott, A. Toschi, H. Ikeda, and K. Held, Wien2wannier: From linearized augmented plane waves to maximally localized Wannier functions, Comput. Phys. Commun. **181**, 1888 (2010).

[28] X. Wang, J. R. Yates, I. Souza, and D. Vanderbilt, *Ab initio* calculation of the anomalous Hall conductivity by Wannier interpolation, Phys. Rev. B **74**, 195118 (2006).

[29] M. Kohmoto, Topological invariant and the quantization of the Hall conductance, Ann. Phys. (NY) **160**, 343 (1985).

[30] The SOC coefficient of the 3*d* shell of atomic Fe is 80 meV; see O. Šipr, M. Košuth, and H. Ebert, Magnetic structure of free iron clusters compared to iron crystal surfaces, Phys. Rev. B **70**, 174423 (2004). The bands in BFPO are hybridized with O 2*p* states, decreasing the effective SOC strength to 40 meV.

[31] L. Nordström and D. J. Singh, Noncollinear Intra-Atomic Magnetism, Phys. Rev. Lett. **76**, 4420 (1996).

[32] See Supplemental Material at http://link.aps.org/supplemental/10.1103/PhysRevB.94.125134 for the band-resolved spin and orbital textures, which show similar behavior as in Fig. 7.

[33] B. Kim, C. H. Kim, P. Kim, W. Jung, Y. Kim, Y. Koh, M. Arita, K. Shimada, H. Namatame, M. Taniguchi, J. Yu, and C. Kim, Spin and orbital angular momentum structure of Cu(111) and Au(111) surface states, Phys. Rev. B **85**, 195402 (2012).

[34] Y. Ren, Z. Qiao, and Q. Niu, Topological phases in two-dimensional materials: A brief review, Rep. Prog. Phys. **79**, 066501 (2016).

[35] H. Jiang, Z. Qiao, H. Liu, and Q. Niu, Quantum anomalous Hall effect with tunable Chern number in magnetic topological insulator film, Phys. Rev. B **85**, 045445 (2012).